SN Computer Science (2023) 4:100
https://doi.org/10.1007/s42979-022-01519-w

ORIGINAL RESEARCH

Novel Programmable Readout Amplifier and Potentiostat for Glucose Sensing Applications

Riyaz Ahmad[1] · Amit M. Joshi[1] · Dharmendar Boolchandani[1] · Tarun Varma[1]

Received: 30 April 2022 / Accepted: 21 November 2022 / Published online: 17 December 2022

Abstract

The paper presents a novel design of programmable current mode readout amplifier and potentiostat circuits for glucose sensing applications. In the proposed design, the threshold voltage of two MOS transistors is used as the reference supply voltage across glucose sensor reference and working electrodes. Another important feature is enhancement of the gain of PTA by transconductance (g_m) boosting technique which is useful to detect sensor currents even if a very small amplitude signal is present. The performance of proposed design is analysed using SCL 0.18 µm CMOS process technology with 1.5 V of power supply. The proposed design have programmable gain ranges from 42.18 to 60.38 dB and it offers a IRN of 1.002 nV/sqrt (Hz)–1.688 µV/sqrt (Hz)@ 1–100 MHz. The % THD ranges from 8.26 to 8.34@ 35 nA to 230 nA of sensor current, high DR of 108 dB and PSRR is 100.4 dB. The linear range is found from 35 to 230 nA for the current of glucose sensor i.e. from 5 to 34 MΩ approximately for electrode resistance of glucose sensor which is acceptable for the measurement of glucose level ranges from 40 $\frac{\text{mg}}{\text{dl}}$ to 250 $\frac{\text{mg}}{\text{dl}}$. The power dissipation of the proposed architecture ranges from 165.11 to 459.50 µWatt.

Keywords Electrochemical sensor · Glucose measurement · Potentiostat · Current-conveyor (CC) · g_m boosting · PTA logic control

Abbreviations

PTA	Programmable transconductance amplifier
SCL	Semiconductor Laboratory
IRN	Input referred noise
THD	Total harmonic distortion
DR	Dynamic range
PSRR	Power supply rejection ratio
RE	Reference electrode
WE	Working electrode
CE	Counter electrode
CM	Current mode
VM	Voltage mode
TIA	Transimpedance amplifier
CC	Current-conveyor
UGB	Unity gain bandwidth
PSD	Power spectral density
IC	Inversion coefficient

List of Symbols

g_m	Transconductance
k_n	Transconductance parameter
μ_n	Mobility of NMOS transistor
c_{ox}	Oxide capacitance of transistor
V_{TH}	Threshold voltage
α_c	Current tracking error
I_{oj}	Output current of PTA at various value of j
V_{oj}	Output voltage of readout at various value of j
S_{VIN}	Power spectral density of input-referred thermal-noise voltage
k	Boltzman's constant
n	Substrate factor

Amit Mahesh Joshi, Dharmendar Boolchandani and Tarun Varma have contributed equally to this work.

This article is part of the topical collection "Smart and Connected Electronic Systems" guest edited by Amlan Ganguly, Selcuk Kose, Amit M. Joshi and Vineet Sahula.

✉ Riyaz Ahmad
2018rec9120@mnit.ac.in

Amit M. Joshi
amjoshi.ece@mnit.ac.in

Dharmendar Boolchandani
dboolchandani.ece@mnit.ac.in

Tarun Varma
tvarma.ece@mnit.ac.in

[1] Department of Electronics and Communication Engineering, Malaviya National Institute of Technology, Jaipur, Rajasthan 302017, India

T Temperature in kelvin
Γ Thermal-noise factor

Introduction

Diabetes is a disorder that occurs when the human body has difficulty maintaining blood glucose levels. Diabetes is a chronic condition characterised by elevated blood glucose levels within the human body [1]. The primary cause of diabetes is an imbalanced glycemic profile. Diabetes is one of the fastest-growing health problems, with the number of patients with diabetes tripled in the last 2 decades [2]. As a result, diabetic individuals must have their glucose levels monitored on a regular basis [3, 4]. To test body glucose, an electronic interface that can handle glucose concentration levels is required. To perform the daily activities, the body requires glucose, however the normal range of glucose is from (80–150 $\frac{mg}{dl}$) [5, 6]. The higher value of the glucose is hyperglycemia (i.e. Diabetes) and lower glucose levels in the body termed as hypoglycemia [7]. The hypoglycemia may lead to various health problems like kidney failure, blindness, Cardiovascular disease etc [8].

For processing electrochemical sensor (e.g. blood glucose sensor) signals, a potentiostat and readout circuits based electronic interface is useful. For glucose sensing, three electrode electrochemical cells are commonly employed. The RE, WE, and CE are used in glucose sensing employing amperometric sensors, i.e. electrochemical cells [9]. At the WE electrode, the major reaction occurs at a constant reference voltage. The reference voltage generated by the potentiostat circuit maintains a constant voltage between RE and WE electrode while injecting the correct amount of current into CE electrode. A readout circuit processes the current passing through CE, i.e. sensor current. An amplifier, current buffer, current to voltage converter, or a combination of these circuits can be used in a readout circuit. The readout circuit in the proposed architecture amplifies the sensor current and converts it to voltage that is proportional to glucose concentration level. An equivalent circuit model of a glucose sensor is used to interface with a readout and potentiostat circuit to view and process the sensor current in this research paper.

To process electrochemical sensor signals, several systems use VM circuits. Furthermore, CM circuits have a number of advantages over their VM counterparts [10–13]. In addition, CM circuits require less power than VM circuits. For the processing of electrochemical sensor signals, several structures have been developed. The majority of them utilised VM circuitry based on op-amps, with only few of research based on CM circuitry. In the [14], the TIA was utilised with high feedback resistors to process low sensor current, and the WE was not connected to true ground, making it sensitive to external disturbances. As a result, high noise and circuits necessitate a large space.

The switched capacitor based design was more complicated and used a lot of power [15]. The op-amp based compact design based on current mirror in [16] was utilised to detect current. [17] provides a better potential control, but it has several drawbacks [14]. With a complex structure and many passive elements, an enhanced sensing strategy was utilised [18, 19]. Jose et al. [20–22] was useful for measuring a small range of glucose concentration with a higher power dissipation. Complex circuitry was employed in the multichannel readout interface in [23]. Karandikar et al. [24] suggested a compact design that relies on a high load resistance to detect small sensor currents.

The CC based TIA with low gain was reported in [25, 26]. The CM and resistive TIA based readout circuit in [27] was operated relatively at higher power dissipation. The readout interface designs for electrochemical signal detection and system for monitoring of glucose level have been reviewed in [28–32]. The various features of instrument development and application for electrochemical sensor signal processing were discussed [33]. More literature [34–37] were found to evaluate the performance of analog front ends for electrochemical sensors, particularly glucose sensor interfaces. After reviewing the literature [14–27, 34–37], It has been determined that, most of the structures are VM i.e. Op-amp based, which necessitates different external circuitry for the potentiostat i.e. reference voltage generation and readout circuit to change sensor current into corresponding output voltage. Externally generated reference voltage absorbs a lot of power, produces a lot of noise, and adds to the complexity of the construction. The CM is used in only a few constructions.

The novel architecture is proposed and the PTA circuit of readout is also introduced which has programmable features. The proposed design combines a potentiostat and a CM readout circuit into a single circuit. The advantages of proposed design over existing literature are as follows:

- The threshold voltage of two MOS transistors is considered as a reference voltage which obviates the necessity for external reference voltage generation.
- The g_m boosting approach is used to increase the gain of the PTA circuit.
- The circuit is more compact because no op-amp is required.
- The potentiostat and current readout amplifier circuit functions are effectively integrated in the architecture.
- WE terminal is connected to the actual ground, which eliminates noise pickup from the environment.
- The proposed architecture has low noise and consumes low power.

The detailed interface architecture and the proposed potentiostat and readout amplifier circuit for glucose sensing is implemented in CMOS in "Proposed Electronics Interface and Design of Programmable Readout Amplifier Circuit". The results are discussed in "Results and Discussion", comparison of various literature is given in "Comparison" and then finally the paper is concluded in "Conclusion.

Proposed Electronics Interface and Design of Programmable Readout Amplifier Circuit

Potentiostat and a readout amplifier circuit are used to interact with a glucose sensor model in the suggested electronics architecture for glucose concentration measurement. Figure 1 depicts the whole electronic interface design for glucose sensing, which includes a potentiostat, sensor model, and readout circuit.

In Section "CMOS Implementation and Analysis of Potentiostat, a detailed explanation of the proposed potentiostat that generates reference voltage for glucose sensors, as well as an equivalent circuit model of the glucose sensor, is provided, and in Section "CMOS Implementation and Analysis of Programmable Readout Amplifier Circuit, a proposed programmable readout circuit for glucose sensing is presented.

The WE and RE electrodes of the equivalent circuit of a glucose sensor are connected to a potentiostat, which uses the threshold voltage of MOS transistors as a reference voltage. The current flowing through CE terminal which is also termed as sensor current is fed into differential CC to buffer the sensor current effectively as CCs have several advantages over the current mirrors. The sensor current after CC is amplified with the help of PTA which provides current amplification at different levels with help of PTA control circuit and finally the amplified current is converted into voltage with the help of simple NMOS based current to voltage (*I*–*V*) converter.

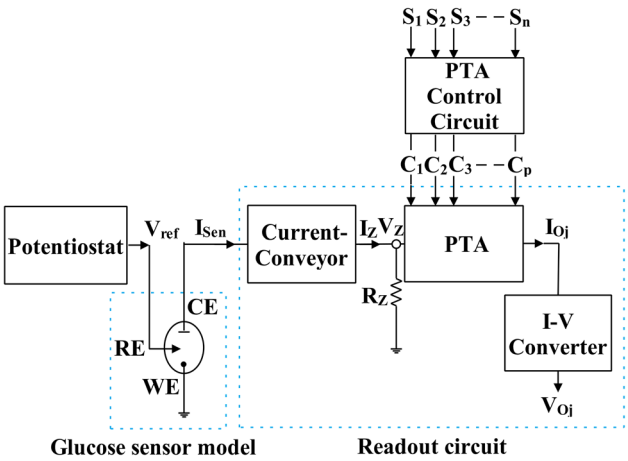

Fig. 1 Block level architecture for glucose monitoring

CMOS Implementation and Analysis of Potentiostat

The potentiostat is a crucial component of the electronic glucose sensing interface because it provides a fixed reference voltage between the sensor's RE and WE terminals. Figure 2 [5] shows the suggested circuit for a potentiostat. The threshold voltages of MOS transistors M8 and M9 provide the required amount of fixed voltage across the RE and WE terminals of the glucose sensor. For 0.18 µm CMOS technology, the NMOS threshold voltage is roughly 0.44 V, hence the summation of the threshold voltages of transistors M8 and M9 serves as a reference voltage.

In comparison to RE, WE, and CE terminal resistances in the resistive equivalent model depicted in Fig. 3, small values of capacitances and small surface resistances are ignored. Fig. 4 shows the analysis of the voltage across RE and WE. The sensor current (I_{sen}) flows through CE and WE terminals during the chemical reaction, hence, a equivalent resistance (R_{eq}) must be there in the route of flow of sensor current. The

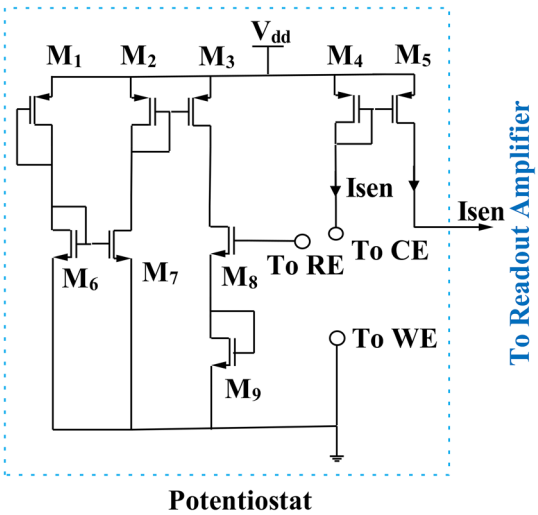

Fig. 2 Potentiostat circuit for fixed reference voltage generation

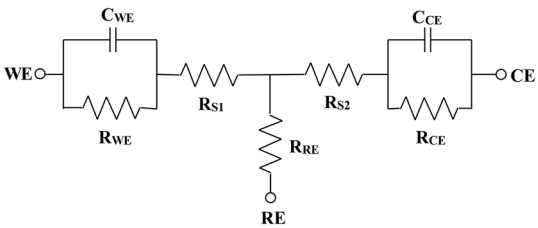

Fig. 3 Glucose sensor equivalent circuit model

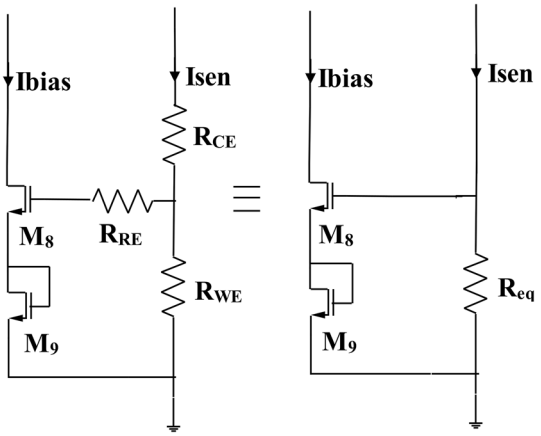

Fig. 4 Sensor current based on a threshold voltage

current passing through R_{eq} the sensor current. As a result, the relationship between I_{sen} and R_{eq} can be expressed as follows:

$$I_{sen} = \frac{V_{GS8} + V_{GS9}}{R_{eq}}. \tag{1}$$

Since,

$$I_{bias} = k_n\left(V_{GS8} - V_{TH}\right)^2. \tag{2}$$

where, I_{bias} is the value of current bias, $k_n = \frac{1}{2}\mu_n C_{ox}\frac{W}{L}$ is the device transconductance parameter of transistors M8 & M9 whereas V_{TH} is the threshold voltage. As a result, V_{GS8} from (2) can be calculated and is specified as:

$$V_{GS8} = V_{TH} + \sqrt{\frac{I_{bias}}{k_n}}. \tag{3}$$

The expression for V_{GS9} can be stated in the same way, with the same bias current I_{bias} flowing through transistor M9. Hence,

$$V_{GS9} = V_{GS8} = V_{TH} + \sqrt{\frac{I_{bias}}{k_n}}. \tag{4}$$

If the I_{bias} is small and $(\frac{W}{L})_8$ and $(\frac{W}{L})_9$ are high enough, the statement inside the square root can be minimized in comparison to V_{TH}, and its value can be ignored. WE terminal resistance (R_{WE}) also plays a significant role in the glucose sensor's chemical reactions, as its value is significantly higher than that of the CE and RE terminals resistance. As a result, the (1) changes to

$$I_{sen} \approx \frac{2V_{TH}}{R_{eq}} \approx \frac{2V_{TH}}{R_{WE}}. \tag{5}$$

The I_{sen} solely depends on R_{eq} or R_{WE}, according to (5), because V_{TH} is constant. Transistors M4 and M5 mirror the sensor current, it is then sent into the readout circuit for further processing and amplification.

CMOS Implementation and Analysis of Programmable Readout Amplifier Circuit

Readout circuit is a very essential part for electrochemical signal amplification and processing. Figure 5 shows the CMOS realization of the readout circuit, which includes a differential CC, PTA, and a basic *I–V* converter. The suggested readout circuit is constructed utilising the g_m/I_D design technique, and the trade-off in analog CMOS design [38] are optimised to make it appropriate for implementing a readout interface circuit for glucose sensing applications.

The important features of proposed readout circuit are as follows:

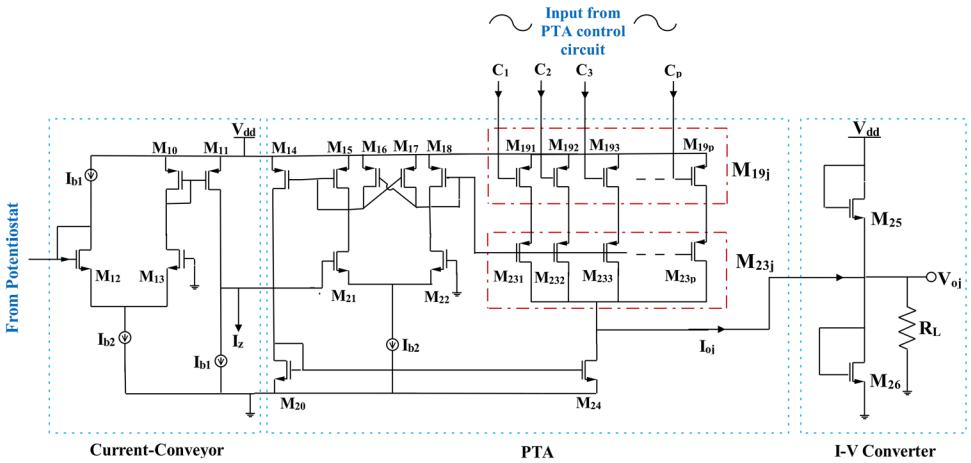

Fig. 5 Read-out circuit for glucose signal detection and amplification

1. A digital control logic circuit is used to obtain different levels of gain of PTA.
2. To reduce drain thermal noise, the lower and upper MOS transistors of differential CC and PTA are retained between the moderate and low side of the strong inversion region.
3. Input devices of differential CC and PTA use MOS transistors that operate between moderate inversion and the low side of weak inversion region. It would help the proposed design to minimize the input pair, input referred thermal noise by maintaining large g_m/I_D or g_m. This allows the device to overcome the readout circuit noise. Because electrochemical sensors are very sensitive, and noise might impact the sensor interface performance, hence noise should be kept to a minimum.
4. For gain enhancement, the CMOS PTA circuit employs partial positive feedback. The partial positive feedback used with cross connected MOSFETs [39], boosts both the DC gain and the UGB. Using cross coupled MOSFETs, the transconductance (g_m) of PTA is improved without raising the bias current which is useful for applications with low power consumption.

The current I_{sen} from the sensor is given to differential CC, resulting in current I_z. The differential CC allows for healthier sensor current buffering and processing. The expression describes the relationship between I_z and I_{sen} is given as

$$I_z = \alpha_c I_{sen}, \tag{6}$$

where, α_c is termed as the current tracking error of differential CC. The α_c will be close to unity value if the z terminal impedance is low in comparison to the output impedance of MOS transistor M5. So,

$$I_z \approx I_{sen}. \tag{7}$$

After differential CC, the PTA block is utilized to amplify the sensor current. the PTA's g_m is increased by connecting cross coupled MOS transistors M16 and M17, which increases the gain of PTA without raising the bias value of current. the PTA's effective value of transconductance G_m can be calculated easily using the DC transfer expression.

$$G_m = \frac{g_{m21}}{1 - \frac{g_{m16}}{g_{m15}}}. \tag{8}$$

According to (8), a large transconductance value can be obtained if the ratio of M16 and M15 transconductance value is kept near to unity. The acronym PTA comes from the fact that the transconductance amplifier has a programmable output terminal, as seen in Fig. 5. PTA control circuit is shown in Fig. 6. For understanding the operation, 8 control signals (C_1, C_2 ...C_8) are generated with the help

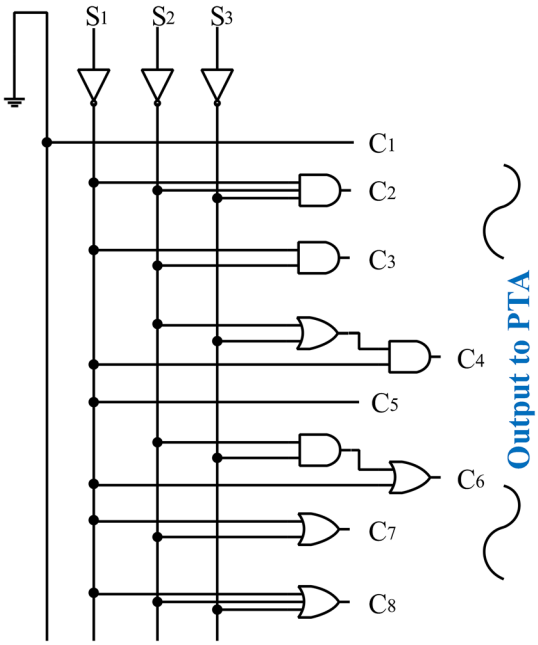

Fig. 6 Programmable transconductance amplifier (PTA) control circuit

of 3 select input lines ((S_1, S_2 and S_3). The truth table for generating control signals is given in Table 1.

The following is a general expression for PTA output current:

$$I_{oj} = jI_o \tag{9}$$

where, $j = 1, 2, 3, \ldots p$, so that the various currents at output, I_{o1}, I_{o2}, I_{o3}...I_{op} of PTA are equal to I_o, $2I_o$, $3I_o$,...,pI_o respectively. The output current I_o (i.e. for $j = 1$) of PTA is expressed as

$$I_o = G_m V_z = G_m R_z I_z, \tag{10}$$

(10) was updated to expression (11) by placing the value of I_o from (6) into (10).

$$I_o = \alpha_c G_m R_z I_{sen}. \tag{11}$$

In (11), the quantity $\alpha_c G_m R_z$ denotes the PTA's current gain. It becomes (12) after changing the value of I_{sen} from (5) into (11).

$$I_o \approx G_m R_z \alpha_c \frac{2V_{TH}}{R_{WE}}. \tag{12}$$

Finally, a simple I–V converter is used to convert I_o to voltage. The output voltage is expressed as

$$V_o = \frac{I_o}{k_n(V_{DD} - V_{TH})} R_L \approx G_m R_z \alpha_c \frac{2V_{TH}}{R_{WE}} (r_{o25} \parallel R_L). \tag{13}$$

Table 1 Truth table of PTA control logic circuit

S_1	S_2	S_3	C_1	C_2	C_3	C_4	C_5	C_6	C_7	C_8
0	0	0	0	1	1	1	1	1	1	1
0	0	1	0	0	1	1	1	1	1	1
0	1	0	0	0	0	1	1	1	1	1
0	1	1	0	0	0	0	1	1	1	1
1	0	0	0	0	0	0	0	1	1	1
1	0	1	0	0	0	0	0	0	1	1
1	1	0	0	0	0	0	0	0	0	1
1	1	1	0	0	0	0	0	0	0	0

Table 2 MOS transistors dimensions of potentiostat and readout circuits

MOS transistors	$\frac{W}{L}$ (µm)	MOS transistors	$\frac{W}{L}$ (µm)
M1	1/0.72	M14–M15,M18	9.32/0.72
M2–M5	9.32/0.72	M16–M17	9.23/0.72
M6–M7	1.8/0.72	M19j	9.32/0.72
M8–M9	10/0.72	M20	1.8/0.72
M10–M11	9.32/0.72	M21–M22	7.12/0.72
M12–M13	7.12/0.72	M23j	45/0.72
		M24–M26	1.8/0.72

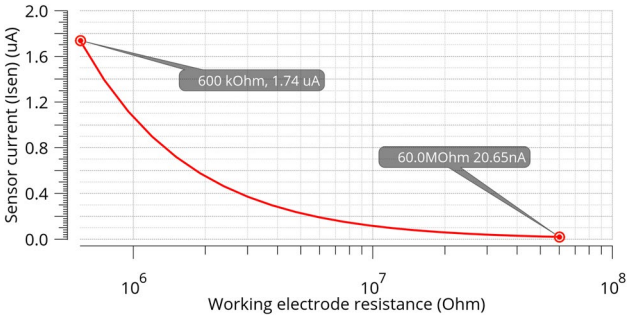

Fig. 7 Relation between sensor current (I_{sen}) and working electrode resistance (R_{WE})

Where, r_{o25} is the *I–V* converter's internal output resistance. In addition, the general expression for readout circuit output voltage can be stated as

$$V_{oj} = I_{oj}\left(r_{o25} \parallel R_L\right) = jV_o \tag{14}$$

According to the (14), the output voltage of glucose measurement is only dependent on the resistance R_{WE}, as other terms are constant. For $j = 1, 2, 3, \ldots p$, the various output voltages V_{o1}, V_{o2}, V_{o3}...V_{op} of readout amplifier are equal to V_o, $2V_o$, $3V_o$,...pV_o respectively.

Results and Discussion

The Cadence Virtuoso simulation software is used to conduct tests on the suggested electronic architecture for glucose level measurement with SCL 0.18 µm CMOS technology. Figures 2 and 5 demonstrate CMOS circuit implementations of potentiostat and readout circuits, respectively. Table 2 shows the size of the MOS transistors used in the proposed design.

For all simulations, the supply voltage of $V_{dd} = 1.5$ V is utilised. The potentiostat circuit is biased, and a continuous voltage of higher than 2 times of V_{TH}, roughly 0.85–1 V, is maintained across the RE and WE terminals of the sensor model. $I_{b1} = 5$ µA and $I_{b2} = 10$ µA are the differential CC and PTA bias currents, respectively. The resistance R_z was set to 11.11 kΩ to ensure that the sensor current was amplified effectively and linearly. The proposed design is suited for measuring glucose concentration levels in the range of 40–250 $\frac{mg}{dl}$, which helps to measure the glucose range of a pre-diabetic, diabetic, hypoglycemia and healthy patient.

The plot shown in Fig. 7 depicts the relationship between sensor current (I_{sen}) flowing through the CE terminal and sensor electrode resistance R_{WE}.

The I_{sen} varies from 1.74 µA to 20.65 nA depending on the resistance R_{WE}, which ranges from 600 kΩ to 60 MΩ. As in a glucose sensor, as the blood glucose concentration rises, the electrode resistance lowers, increasing output current and thus the output voltage.

The PTA's programmable gain is depicted in Fig. 8. We opted to plot 8 gain curve values to maintain the best linearity range, which can be attained by enabling MOS transistor M23*j* (*j*= 1, 2, 3, 4, 5, 6, 7, 8) with the help of PTA control logic signals (C_1, C_2...C_8). The current gain corresponding to $j = 1, 2, 3, 4, 5, 6, 7, 8$ are 42.17, 48.22, 51.76, 54.29, 56.24, 57.85, 59.21 and 60.38 in dB. These gains are constant for R_{WE} ranges from 5 to 34 MΩ, i.e. sensor current varying from 35 to 230 nA, as shown in Fig. 8.

Figure 9 shows the relationship between output voltage of the readout circuit and sensor current. There is a load resistance R_L of value 1 kΩ which is applied to the output of the *I–V* converter to plot this relationship. According to the graph, the proposed readout circuit has a linear range of

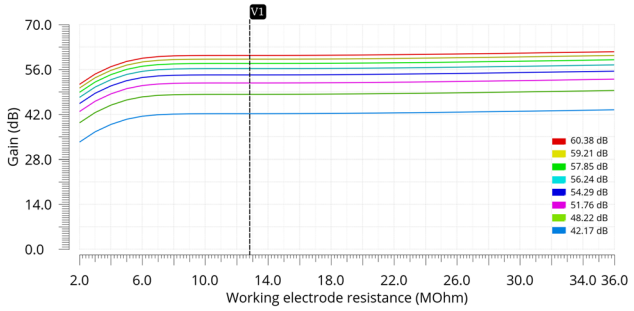

Fig. 8 Gain of programmable transconductance amplifier (PTA)@j = 1, 2, 3, 4, 5, 6, 7, 8

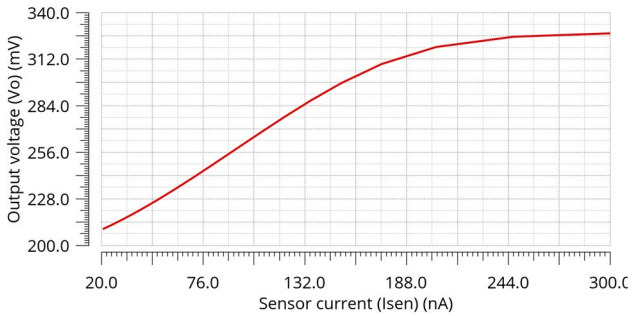

Fig. 9 Relation between output voltage of readout circuit and sensor current

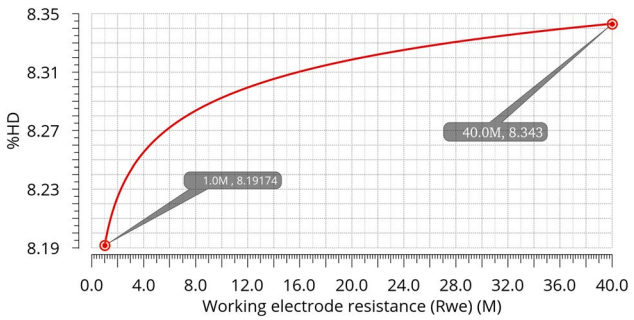

Fig. 10 % Total harmonic distortion

operation from 35 to 230 nA for a matching output voltage from 217.64 to 323.12 mV.

Some more critical analysis has been performed which are discussed in subsequent Sections "%THD and xf Analysis", "Noise Analysis", "Monte Carlo analysis" and "PVT Analysis".

%THD and xf Analysis

The %THD is displayed in Fig. 10 at a fixed fundamental frequency of 1 kHz to understand the effect of distortions on the output voltage of the proposed readout amplifier. The change

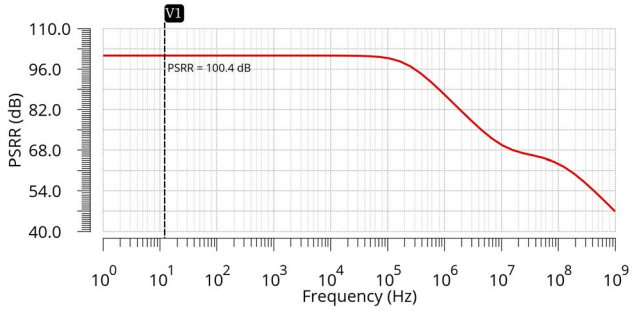

Fig. 11 Power supply rejection ratio

of %THD for different values of sensor working electrode resistance is also observed. For 1–40 MΩ resistance fluctuation, the %THD variation is determined to be in the range of 8.19–8.34%.

The proposed readout circuit noises and disturbance rejection are further tested using the xf analysis against power supply changes. The PSRR has been found to be 100.4 dB and shown in Fig. 11.

Noise Analysis

The noise analysis is carried out on the PTA of the readout circuit. The input devices of PTA are operating between the low side of weak inversion and moderate inversion region ($g_m/I_D \approx 18$) for large g_m/I_D or g_m value to decrease input pair, input referred thermal noise. This aids the device in dominating the PTA noise in general. Then, PTA's contribution to thermal noise is analysed. Figure 5 depicts the PTA portion of the readout circuit. The PSD of the PTA input-referred thermal-noise voltage is expressed as

$$S_{\mathrm{VIN}}(\mathrm{thermal}) = 4kT\left[2\times\frac{(n\Gamma)_{21}}{g_{\mathrm{m21}}} + 2\times\frac{(n\Gamma)_{20}g_{\mathrm{m20}}}{g^2_{\mathrm{m21}}} + 2\times\frac{(n\Gamma)_{15}g_{\mathrm{m15}}}{g^2_{\mathrm{m21}}} + p\times\frac{(n\Gamma)_{18}g_{\mathrm{m18}}}{g^2_{\mathrm{m21}}}\right] \quad (15)$$

g_{m21}, g_{m20}, g_{m15}, and g_{m18} are transconductance for the input differential pair transistors M21 and M22, non-input transistors i.e. current-mirror devices M20 and M24, M14 and M15, M18 and M23j, respectively. The products of the substrate factor, n, and thermal-noise factor, Γ corresponds to $(n\Gamma)_{21}$, $(n\Gamma)_{20}$, $(n\Gamma)_{15}$ and $(n\Gamma)_{18}$ of transistors M21, M20, M15 and M18 respectively. Because current mirror pair devices are employed throughout the signal path, the factor "2 and p" occurs in the noise expression. The gate referred thermal-noise voltage PSD of the input differential pair devices is the first term in (15). The second, third, and fourth terms correspond to the non-input, current-mirror device's drain-referred thermal-noise voltage PSD, with each term divided by the square of the transconductance, $g^2{}_{m21}$ of input

pair devices. In [38], the relationship between IC and g_m is described as,

$$g_{\mathrm{m}} = \frac{I_{\mathrm{D}}}{nV_T\sqrt{\left(\mathrm{IC} + 0.5\sqrt{\mathrm{IC}} + 1\right)}}. \tag{16}$$

According to (15), a large g_{m} of input pair devices M21 and M22 decreases thermal-noise since it is inversely proportional to all noise components. As a result, while operating non-input devices at moderate inversion for moderate g_{m}, the g_{m} boosting technique is helpful to decrease contribution of the thermal noise of PTA, as the effective value of g_{m} increases. The IRN response is shown in Fig. 12. It's value ranges from 1.002 nV/sqrt(Hz) to 1.688 µV/sqrt(Hz)@1 Hz–100 MHz.

Monte Carlo Analysis

Monte Carlo analysis is used to verify the robustness of the suggested readout amplifier. Monte Carlo simulations are run with a random sample distribution (500 samples) and a 5% mismatch. The Monte Carlo simulation has been conducted for 500 samples run and Gaussian random variations has been specified for varying the %THD at sensor working electrode resistance of 10 MΩ. The mismatch effect can be seen on the %THD in Fig. 13. As a result, the suggested potentiostat and readout circuit designs are resilient and are proved to be satisfactory even when device parameters are changed. For %THD, the mean and standard deviations are 8.293 and 74.713 m, respectively.

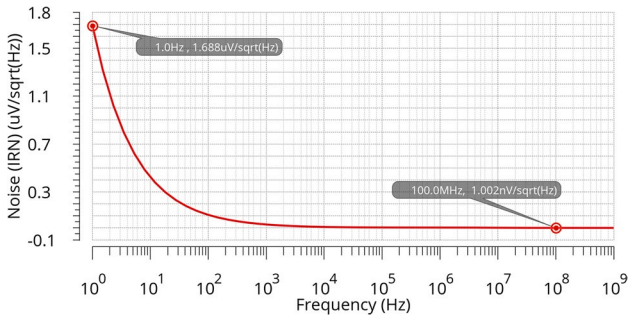

Fig. 12 Input referred output noise

PVT Analysis

PVT study has been also carried out to see if the parameters of the proposed architecture differed in any way. Slow-slow, slow-fast, typical-typical, fast-slow, and fast-fast are investigated for process variation. The gain, PSRR, power consumption, and %THD parameters are examined for $j = 1, 2, 3, 4, 5$ (i.e. 5 transistors are ON at a time) by adjusting the power supply voltage ±5% and temperature ranges from $-40\,^{\circ}C$ to $100\,^{\circ}C$ in $20\,^{\circ}C$ steps. Tables 3 and 4 exhibit the simulated findings of the PVT analysis. The effect of variation of process corner on gain, PSRR, power consumption, and %THD is insignificant, as shown in Table 3. The maximum deflection due to voltage variation is observed around 2% on gain, 16% on PSRR, 22% on power dissipation and 28% on %THD. Also, From Table 4 it is observed that the maximum deflection due to variation in temperature is around 2.5% on gain, 4% on PSRR, 3% on power dissipation and 26% on %THD.

A DR can be evaluated using (17), in which I_{sen} is the maximum input to PTA at a particular gain value of 60.38 dB (= 1044) and I_{noise} is noise level. For $I_{\mathrm{sen}} = 230$ nA, Gain = 60.38 dB, and $I_{\mathrm{noise}} = 1.002$ nA, A DR of 108 dB can be obtained.

$$\mathrm{DR} = 20 \times log_{10}\left(\mathrm{Gain} \times \frac{I_{\mathrm{sen}}}{I_{\mathrm{noise}}}\right) \tag{17}$$

Several simulations have been conducted to test the suggested design's performance parameters, which are listed in Table 5.

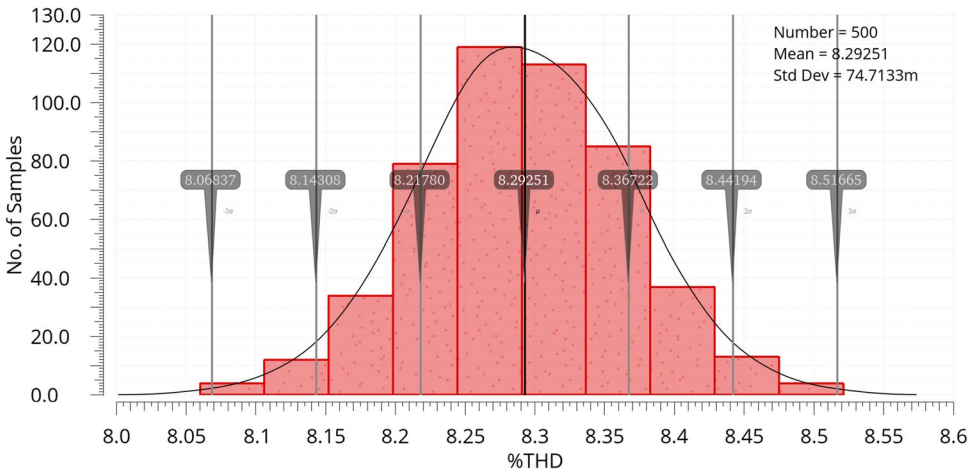

Fig. 13 Monte Carlo simulation of %THD

Although the proposed design has several advantages, some limitations are also there. The proposed readout circuit has a limited range of output voltage. The actual power dissipation might be larger when current from the real glucose sensor feeds to the readout circuit. The readout circuit has a limited but sufficient range of glucose concentration measurement.

Comparison

Table 6 compares the performances of the proposed design to that of the existing literature. A very high power dissipation is reported in [17, 21, 22] and the comparatively low gain is achieved in [25, 26]. The literature [17, 19, 21] shows the higher value of IRN. Power dissipation in [19] was small but it offers low value of dynamic range in comparison to proposed design. As can be seen from the findings, the proposed design has the highest DR, uses the least amount of power dissipation, and is the only one with programmable features. The number of resistors (R), the number of capacitors (C) and the number of MOS transistors used in various literature are also compared. From Table 6, it is observed that there is no capacitor used in proposed design and the number of resistors used are low compared to designs given in [17, 21, 27]. The number of MOS transistors utilised in proposed circuits are lower than circuits in [17, 19, 21, 22, 25]. The less number of passive components and MOS transistor leads to comparatively less power consumption and small core area of the design which also makes the circuit less noisy. The most of the literature used for glucose sensing utilises op-amp based circuits i.e VM circuit while proposed circuit works on CM.

Table 3 Effect of process and voltage variations on the performance of proposed readout amplifier circuit

Parameters	Process variations (V_{dd} = 1.5 V, temp = 27 C)					Supply voltage variations (V_{dd}) (temp = 27 C, process = tt)				
	ss	sf	tt	fs	ff	1.35 V	1.425 V	1.5 V	1.575 V	1.65 V
Gain (dB)	56.06	56.17	56.12	56.14	56.19	57.27	56.69	56.12	55.57	55.02
PSRR (dB)	100.11	101.2	100.4	100.85	101.24	117.2	108.3	100.4	96.65	93.94
Power dissipation (µW)	316.59	317.86	317.5	317.74	318.35	256	286.2	317.5	351.8	389.7
% THD	8.22	8.34	8.29	8.31	8.38	10.66	9.46	8.29	7.16	6.08

Table 4 Effect of temperature variations on the performance of proposed readout amplifier circuit

Parameters	Temperature variations (T) (V_{dd} = 1.5 V, process = tt)							
	– 40 °C	– 20 °C	0 °C	20 °C	40 °C	60 °C	80 °C	100 °C
Gain (dB)	57.62	57.13	56.68	56.26	55.88	55.52	55.21	54.95
PSRR (dB	98.33	98.93	99.63	100.1	101.2	102.2	103.2	104.3
Power dissipation (µW)	306.8	310.4	315.2	317.2	318.2	319.1	319.9	320.7
%THD	6.38	6.82	7.23	7.69	8.54	9.06	9.78	10.43

Table 5 Summary of results of proposed design

Parameters	Simulated values
Process technology	0.18 µm CMOS, SCL
Power supply	1.5 V
Linearity range	I_{sen} = 35–230 nA, R_{WE} = 5–34 MΩ Suitable for 40 $\frac{mg}{dl}$ to 250 $\frac{mg}{dl}$ concentration level measurement
Gain	42.17–60.38 dB @ j = 1, 2, 3, 4, 5, 6, 7, 8
PSRR	100.4 dB
%THD	8.26–8.34@ R_{WE} = 5–34 MΩ
DR	108 dB
IRN	1.002 nV/sqrt(Hz)–1.688 uV/sqrt(Hz)@ 1 Hz–100 MHz
Power dissipation	165.11–459.50 µW

Table 6 Comparison of proposed design with existing literature

References	Process (µm)	Power supply	Input current	Gain	IRN ($/\sqrt{Hz}$)	DR (dB)	Power dissipation	No. of R, C	No. of Transistors	Prog. feature
[17]	0.18	1.8 V	1.4 mA	90 dB	2.5 mV	63	15.84 mW	12, 2	216	NO
[19]	0.18	1.8 V	1.28 µA	5 MΩ	6.5 uV	68	105 µW	1, 5	67	NO
[21]	0.35	1.65 V	5 µA	44.3 kΩ	6.6 mV	NA	5.1 mW	3, 3	53	NO
[22]	0.35	3.3 V	20 µA	42 kΩ	0.47 pA	NA	9.3 mW	1, 12	48	NO
[25]	0.5	5 V	16 µA	30.1 dB	0.14 pA	54	241 µW	1, 3	60	NO
[26]	0.5	3.3 V	50 µA	23.52 dB	0.54 nV	87.5	280 µW	2, 3	29	NO
[27]	0.18	1.8 V	500p–10 µA	NA	NA	86	1.25 mW	4, 4	38	NO
This work	0.18	1.5 V	35–230 nA	42.2–60.4 dB	1.002 nV	108	165.1–459.5 µW	2, 0	39	YES

Conclusion

A novel programmable electronics interface design for glucose sensing application is proposed in this paper. The SCL, 0.18 μm CMOS process technology is used to verify the performance results in Cadence Virtuoso. Various simulations have been run to support the suggested design, and the findings are well-suited for glucose concentration measurements ranging from 40 to 250 $\frac{mg}{dl}$. %THD of around 8% is obtained and also a good value of PSRR and high DR of 108 dB is achieved. The bio signals with small magnitude found in blood glucose can be detected with a programmed gain of 42.17–60.38 dB. Other objects such as tear, uric acid, and so on used in electrochemical sensing applications, can also benefit from such interface designs.

Acknowledgements The authors are grateful to SMDP-C2SD Lab, MNIT Jaipur for providing the support of EDA Tools to conduct the experiments. The PhD scheme of TEQIP-III project under National Project Implementation Unit, MoE, Govt. of India and World Bank supported this research in part.

Data Availability Statement The datasets generated during and/or analysed during the current study are available from the corresponding author on reasonable request.

Declarations

Conflict of Interest The authors declare that they have no conflict of interest.

References

1. Joshi AM, Jain P, Mohanty SP, Agrawal N. iglu 2.0: a new wearable for accurate non-invasive continuous serum glucose measurement in iomt framework. IEEE Trans Consum Electron. 2020;66(4):327–35.
2. Yu Y, Huang J, Zhu J, Liang S. An accurate noninvasive blood glucose measurement system using portable near-infrared spectrometer and transfer learning framework. IEEE Sens J. 2021;21(3):3506–19. https://doi.org/10.1109/JSEN.2020.3025826.
3. Jain P, Joshi AM, Agrawal N, Mohanty S. iglu 2.0: a new non-invasive, accurate serum glucometer for smart healthcare. 2020; arXiv preprint arXiv:2001.09182.
4. Freckmann G, Pleus S, Grady M, Setford S, Levy B. Measures of accuracy for continuous glucose monitoring and blood glucose monitoring devices. J Diabetes Sci Technol. 2019;13(3):575–83.
5. Ahmad R, Joshi AM, Boolchandani D, Varma T. Design of potentiostat and current mode read-out amplifier for glucose sensing. In: 2021 IEEE International Symposium on Smart Electronic Systems (iSES)(Formerly iNiS), 2021; pp. 64–69. IEEE.
6. Joshi AM, Shukla UP, Mohanty SP. Smart healthcare for diabetes during covid-19. IEEE Consum Electron Mag. 2020;10(1):66–71.
7. Bequette BW, Cameron F, Buckingham BA, Maahs DM, Lum J. Overnight hypoglycemia and hyperglycemia mitigation for individuals with type 1 diabetes: how risks can be reduced. IEEE Control Syst Mag. 2018;38(1):125–34.
8. Joshi AM, Jain P, Mohanty SP. iglu 3.0: a secure noninvasive glucometer and automatic insulin delivery system in iomt. IEEE Trans Consum Electron. 2022;68(1):14–22. https://doi.org/10.1109/TCE.2022.3145055.
9. Bard AJ, Faulkner LR. Fundamentals and applications. Electrochem Methods. 2001;2(482):580–632.
10. Yuan F. Voltage-mode versus current-mode: a critical comparison. In: CMOS current-mode circuits for data communications. Analog circuits and signal processing. Boston, MA: Springer; 2007, p. 1–12. https://doi.org/10.1007/978-0-387-47691-9_1.
11. Ahmad R, Joshi A, Boolchandani D. A novel instrumentation amplifier with high tunable gain and cmrr for biomedical applications. Turk J Electric Eng Comput Sci. 2022;30(3):996–1015.
12. Ferri G, Guerrini NC. Low-voltage low-power cmos current conveyors. Springer Science & Business Media; 2003.
13. Tripathi, SK, Ansari MS, Joshi AM. Carbon nanotubes-based digitally programmable current follower. VLSI Des. 2018;2018. https://doi.org/10.1155/2018/1080817
14. Busoni L, Carla M, Lanzi L. A comparison between potentiostatic circuits with grounded work or auxiliary electrode. Rev Sci Instrum. 2002;73(4):1921–3.
15. Zhang J, Trombly N and Mason A. A low noise readout circuit for integrated electrochemical biosensor arrays. In: SENSORS, 2004 IEEE, vol. 1. 2004; pp. 36–39. https://doi.org/10.1109/ICSENS.2004.1426093.
16. Ahmadi MM, Jullien GA. Current-mirror-based potentiostats for three-electrode amperometric electrochemical sensors. IEEE Trans Circ Syst I Regul Pap. 2008;56(7):1339–48.

17. Martin SM, Gebara FH, Strong TD, Brown RB. A fully differential potentiostat. IEEE Sens J. 2009;9(2):135–42.
18. Aleeva Y, Maira G, Scopelliti M, Vinciguerra V, Scandurra G, Cannata G, Giusi G, Ciofi C, Figa V, Occhipinti LG. Amperometric biosensor and front-end electronics for remote glucose monitoring by crosslinked pedot-glucose oxidase. IEEE Sens J. 2018;18(12):4869–78.
19. Xie C, Ma Y, Tang Z, Zhang M. Design of a 68 dB input dynamic range potentiostat for electrochemical biosensing. In: 6th International conference on integrated circuits and microsystems (ICICM), 2021, pp. 426–429. https://doi.org/10.1109/ICICM54364.2021.9660272.
20. Jose PSH, Rajasekaran K, Rajalakshmy P, Jebastina B. A non-invasive method for measurement of blood glucose using bio impedance technique. In: 2nd International conference on signal processing and communication (ICSPC), 2019; p. 138–142. https://doi.org/10.1109/ICSPC46172.2019.8976732.
21. Shenoy V, Jung S, Yoon Y, Park Y, Kim H, Chung H-J. A cmos analog correlator-based painless nonenzymatic glucose sensor readout circuit. IEEE Sens J. 2014;14(5):1591–9.
22. Ghoreishizadeh SS, Taurino I, De Micheli G, Carrara S, Georgiou P. A differential electrochemical readout asic with heterogeneous integration of bio-nano sensors for amperometric sensing. IEEE Trans Biomed Circ Syst. 2017;11(5):1148–59.
23. Hanitra IN, Criscuolo F, Pankratova N, Carrara S, De Micheli G. Multichannel front-end for electrochemical sensing of metabolites, drugs, and electrolytes. IEEE Sens J. 2019;20(7):3636–45.
24. Karandikar N, Jung S, Sun Y, Chung H-J. Low power, low noise, compact amperometric circuit for three-terminal glucose biosensor. Analog Integr Circ Sig Process. 2016;89(2):417–24.
25. Li H, Boling CS, Mason AJ. Cmos amperometric adc with high sensitivity, dynamic range and power efficiency for air quality monitoring. IEEE Trans Biomed Circ Syst. 2016;10(4):817–27.
26. Esparza-Alfaro F, Pennisi S, Palumbo G, Lopez-Martin AJ. Low-power class-ab cmos voltage feedback current operational amplifier with tunable gain and bandwidth. IEEE Trans Circ Syst II Express Briefs. 2014;61(8):574–8.
27. Wang W-S, Kuo W-T, Huang H-Y, Luo C-H. Wide dynamic range cmos potentiostat for amperometric chemical sensor. Sensors. 2010;10(3):1782–97.
28. Jain P, Joshi AM, Mohanty SP. iglu: an intelligent device for accurate noninvasive blood glucose-level monitoring in smart healthcare. IEEE Consum Electron Mag. 2019;9(1):35–42.
29. Wilkins E, Atanasov P. Glucose monitoring: state of the art and future possibilities. Med Eng Phys. 1996;18(4):273–88.
30. Jain P, Joshi AM, Mohanty SP. iglu 1.1: towards a glucose-insulin model based closed loop iomt framework for automatic insulin control of diabetic patients. In: IEEE 6th world forum on internet of things (WF-IoT), 2020; p. 1–6. https://doi.org/10.1109/WF-IoT48130.2020.9221132.
31. Ghosal S, Kumar A, Udutalapally V, Das D. glucam: smartphone based blood glucose monitoring and diabetic sensing. IEEE Sens J. 2021;21(21):24869–78.
32. Jain P, Joshi AM, Mohanty SP. iglu 1.0: an accurate non-invasive near-infrared dual short wavelengths spectroscopy based glucometer for smart healthcare. 2019; arXiv preprint arXiv:1911.04471
33. Lu S-Y, Shan S-S, Lu T-H, Yeh Y-H, Guo S-Z, Chen Y-C, Liao Y-T. A review of CMOS electrochemical readout interface designs for biomedical assays. IEEE Sens. J. 2021;21(11):12469–83. https://doi.org/10.1109/JSEN.2021.3056443.
34. Ahmadi MM, Jullien GA. A wireless-implantable microsystem for continuous blood glucose monitoring. IEEE Trans Biomed Circ Syst. 2009;3(3):169–80.
35. Kuo P-Y, Chen Y-Y. A novel low unity-gain frequency and low power consumption instrumentation amplifier design for ruo2 uric acid biosensor measurement. IEEE Trans Instrum Meas. 2021;70:1–9.
36. Hsiao Y-M, Shiau M-S, Li K-H, Hou J-J, Hsu H-S, Wu H-C, Liu D-G. Design a bioamplifier with high cmrr. VLSI Des. 2013;2013:210265–1.
37. Puttananjegowda K, Thomas S. A low-power low-noise multistage transimpedance amplifier for amperometric based blood glucose monitoring systems. Analog Integr Circ Sig Process. 2020;102(3):659–66.
38. Binkley DM. Tradeoffs and optimization in analog cmos design. In:14th International conference on mixed design of integrated circuits and systems, 2007; p. 47–60. https://doi.org/10.1109/MIXDES.2007.4286119.
39. Wang R, Harjani R. Partial positive feedback for gain enhancement of low-power CMOS OTAs. In: Serdijn W, editor. Low-Voltage Low-Power Analog Integrated Circuits, vol. 328. Boston, MA: Springer; 1995. p. 21–35. https://doi.org/10.1007/978-1-4615-2283-6_3.